Environ Earth Sci
DOI 10.1007/s12665-014-3367-6

ORIGINAL ARTICLE

Conservational use of remote sensing techniques for a novel rainwater harvesting in arid environment

Mohamed Elhag · Jarbou A. Bahrawi

Received: 30 October 2013 / Accepted: 17 May 2014

Abstract Remote sensing applications in water resources management are becoming an essential asset in all different levels of integrated water rational use. Due to remote sensing data availability and different acquisition sensors of satellite images, a wide variability of benchmarks could be conducted under the same theme. Rainwater harvesting is the branch of science where the rainwater is the main target to improve groundwater recharge, stratocumulus clouds are the main source of rain in arid regions. Cloud detection using remote sensing techniques proved to be efficient recently but the general uses of different cloud detection techniques are to precisely omit clouds from satellite images. The use of cloud detection scheme described herein is designed for the MERIS Level1B data; therefore, total set of 60 MERIS images was collected on monthly basis for 5 years started from January 2008. The use of the cloud detection algorithm is to find proper land cover suitable for rainwater harvesting mostly covered with cloud all over the year. Evaluation of land use for rainwater harvesting in terms of groundwater recharge is considered, several factors were taken into consideration and NDWI is one of the most important factors involved. Results pointed out that some regions in southern Saudi Arabia are qualified enough to be considered as potential sites for better rainwater harvesting.

M. Elhag (✉) · J. A. Bahrawi
Department of Hydrology and Water Resources Management, Faculty of Meteorology, Environment and Arid Land Agriculture, King Abdulaziz University,
P.O. Box 80208, Jeddah 21589, Saudi Arabia
e-mail: melhag@kau.edu.sa

Keywords Cloud detection · Geographical information system · MERIS images · Rainwater harvesting · Remote sensing

Introduction

Adequate water management is founded on understanding the interconnections in the hydrological cycle. Informative knowledge of the designated catchment water balance is needed (Elhag et al. 2011). Catchment area by definition is the total area of terrestrial which catches rainfall and contributes the placid water to a certain surface water or potential groundwater recharge (Prada et al. 2009, 2010).

Measurements of water vapor and cloud are important for accurate precipitation forecasts, for estimating surface energy budgets and advance water resources management. In global climate models, a modest error in predicted cloud cover could change the sing of global warming signal (Deepika et al. 2013). Data are needed on the horizontal and vertical distribution of clouds, their scaling properties and cloud microphysical properties.

Humidity measurements are important, especially in the lower troposphere, where shortwave space-based measurements systems have difficulty in penetrating (Engelhardt et al. 2013). While, longwave space-based measurements including thermal infrared can meet the requirements to penetrate clouds. However, horizontal distributions of cloud and in cloud spatial distributions are important parameters that are not presently well measured (Jedlovec et al. 2008; Feister et al. 2010).

The formulation of cloud water is based on the interception befalls of droplets amalgamate on different earth surface features including mainly the vegetation cover (Bruijnzeel et al. 2005; Holder 2003, 2004; Prada et al.

Published online: 01 June 2014

2009; Brauman et al. 2010). Several elements stimulus the formation of cloud water interception including cloud spatial distribution, droplet size, vegetation cover and wind velocity are the basically encountered. Cloud interception by the mountains belt in the study area is expected to be a joint phenomenon along the area (Elhag and Bahrawi 2014).

Soil moisture is important for water resources management. In particular, soil moisture regulates the partitioning of incoming radiative energy into sensible and latent heat fluxes make it relevant to the decision makers (Moghadas et al. 2013). It also partitions precipitation between infiltration, runoff and evaporation, making it equally important for sustainable water resource management. Both of active and passive microwave systems have been used to estimate soil moisture remarkably (Dasgupta 2007; Moghadas et al. 2013).

Groundwater is becoming a more important source of water in many years. Unfortunately, the last decade witnesses an over exploitation of groundwater, in a whole or in part, over recharge (Al-Othman and Ahmed 2012; Huang et al. 2013). Methods for inventorying groundwater, for assessing changes in its availability and for reliable predictions of future change and need for effective groundwater management (Al-Charideh 2012; Deepika et al. 2013).

The impact of lithology and geomorphology in semiarid regions is exemplified by variances between designated areas and its adjoining geological feature (Gieske 1992; De Vries 1997; Selaolo 1998; De Vries et al. 2000). Sinkhole in Saudi Arabia receives about 47 % of the average rainfall (100 mm/year) and withdraws surface runoff into its sinkholes interconnections (Hoetzl 1995).

Medium resolution imaging spectrometer (MERIS) imagery is used in the current research. Two of the key features of the MERIS instrument are its temporal resolution (revisit time of 3 days) and it's spatial coverage (swath width of 1,150 km) with spectral range from 400 to 1,000 nm, which make unavoidable the presence of cloud covers (Delwart et al. 2007; Brockmann et al. 2011).

The aim of the current study is to improve rainwater harvesting in terms of groundwater recharge through: (1) create spatiotemporal cloud map, (2) evaluating delineated watershed lies beneath mostly cloudy area all year round and (3) adequate condition of soil moisture and geological map.

Materials and methods

Study area

Study area located between the Red Sea on the west and Najd Plateau and the Empty Quarter on the east. Mountains belt are located adjacently to the Red Sea side and positioned vertically from North to South (Fig. 1). Investigated area is about 100,000 km^2 of Red Sea coastal plains, high mountains, and the upper valleys of the wadis (seasonal watercourses) are Bīshah and Tathlīth. Agricultural practices are undergoing on a prosperous scale within the region. It has an area of 77,088 km^2 and an estimated population of 1,563,000. The western slope of the designated study area escarpment is steep with relatively short wadi systems. On the other hand, the area to the east of the escarpment is characterized by large catchments with a milder slop and longer wadi system. The average annual rainfall in the highlands probably ranges from 600 to 10,000 mm falling in two rainy seasons, the chief one being in March and April with some rain in the summer. Meanwhile, the eastern plains and plateaus receive much lower amounts, from 500 mm to below 100 mm. Diurnal temperature variations are extreme in the highlands, and considered to be the greatest in the world. It is common for afternoon temperatures to be over 30 °C, yet mornings can be frosty and fog can cut visibility to near 0 %. As a result, there is much more natural vegetation in the study area than in any other part of Saudi Arabia. The geology of the study area contains different geological features including: the mountains consist primarily of sedimentary rock, limestone, sandstone and shale, of Jurassic, Cretaceous and Paleogene origin on a Precambrian granitic basement (El-Maghraby et al. 2013).

Methodological framework and dataset

The current research study is founded on the interconnections of different aspects or research prospective.

Cloud detection algorithm was implemented to produce cloud certainty thematic maps over the designated study area using 60 imageries collected from January 2008 till December 2013 on monthly basis, satellite imageries were collected from MERIS instrument on board the European Space Agency (ESA) ENVISAT environmental satellite. Soil moisture content was evaluated using Landsat 8 image collected after the rainy season in June 2013. Morphometric maps such as slope, aspect and hillshade were generated based on ASTER Digital Elevation Model. To estimate potential flow direction, basin areas and streams flow, and watershed delineation were needed.

Cloud detection algorithm

The cloud detection scheme described herein is designed for the MERIS Level1B data and is based on inverse modeling of radiative transfer simulations covering the natural variability of spectral cloud and surface properties. The simulated radiances have been used to train an artificial neural network (ANN) to discriminate between the

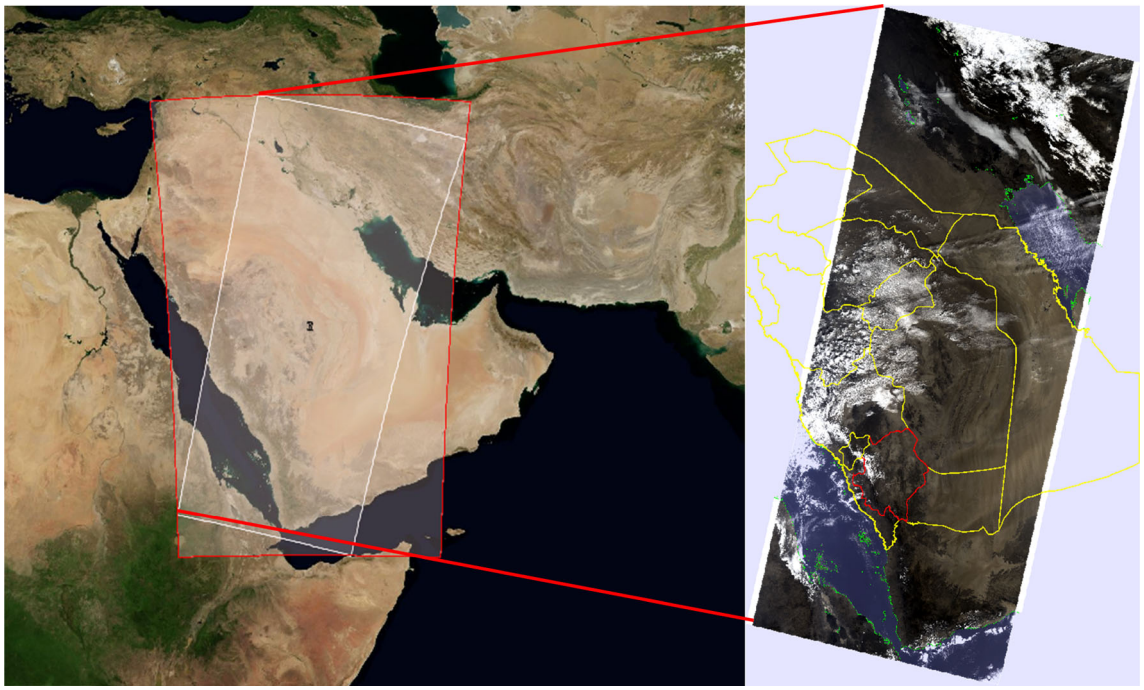

Fig. 1 Administrative boundaries of KSA regions with location of the study area highlighted

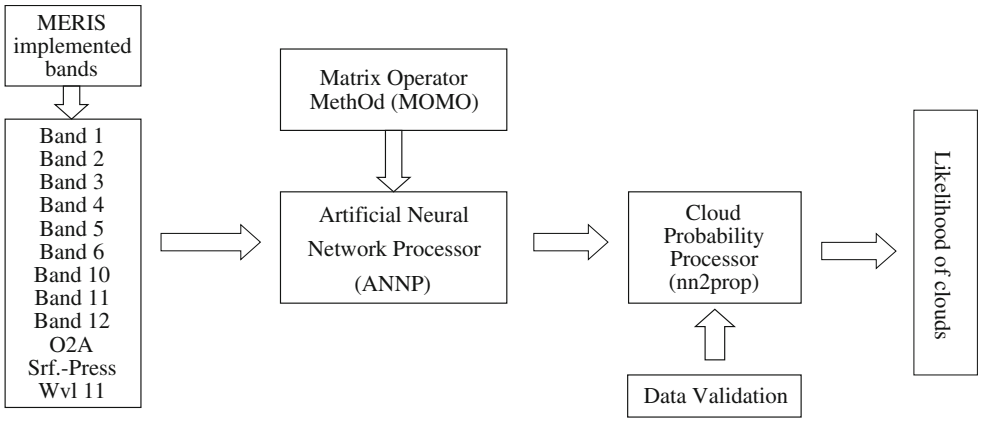

Fig. 2 MERIS cloud detection algorithm

cloudy and cloud free cases (Weaver et al. 2001; Kazantzidis et al. 2012). The cloud detection algorithm is using nine spectral bands of MERIS. Specifically, the ratio of band 10 (cloud optical thickness, cloud-top pressure reference), band 11 (Cloud-top/Surface pressure) and band 12 (aerosol, vegetation) which is an oxygen absorption indicator (Rink et al. 2012). Algorithm yields a probability value (0–1) indicating if a pixel can be regarded as a cloud or not (Fig. 2). Such a probability permits a more flexible way to work with identified clouds compared to a binary cloud mask (McNally and Watts 2003; Lindstrot et al. 2009). The algorithm uses two different artificial neural networks. During development of the algorithm by Fischer and Grassl (1984), Fell and Fischer (2001), using the radiative transfer model MOMO (matrix operator method), simulated cloud and noncloud top of atmosphere radiance have been produced and an artificial neural net has been trained (Saunders and Kriebel 1988; Mecikalski et al. 2011). A post-processing is applied after the net (nn2prop) which scales the output of the artificial neural network into a probability value.

Cloud detection algorithm validation

There different levels of validation were implemented to define the more adequate methodology to classify cloudy pixels. Cloudy probability, total ozone concentration and relative humidity are three different masks used to evaluate algorithm outputs. However, the method must work under many situations. Therefore, TOA reflectance is estimated

to remove the dependence on particular illumination conditions (day of the year and angular configuration) and illumination effects due to rough terrain (cosine correction). The irradiance correction corrects the variation of the solar irradiance, which is different between the wavelength of the pixel and the reference wavelength:

$$L_{\mathrm{corr,irr}}(\lambda_0) = L_{\mathrm{meas,pixel}}(\lambda_0) \times \frac{F_{0,\mathrm{ref}}(\lambda_0)}{F_{0,\mathrm{pixel}}(\lambda_0)} \quad (1)$$

The reflectance correction is interpolating along the slope of the reflectances between adjacent wavelengths "λ" from the pixel-wavelengths to the reference wavelength:

$$L_{\mathrm{corr,ref}}(\lambda_0) = \left[L_{\mathrm{meas,pixel}}(\lambda_2) \times \frac{F_{0,\mathrm{ref}}(\lambda_0)}{F_{0,\mathrm{ref}}(\lambda_1)} - L_{\mathrm{meas,pixel}}(\lambda_1) \times \frac{F_{0,\mathrm{ref}}(\lambda_0)}{F_{0,\mathrm{ref}}(\lambda_1)}\right] \times \frac{(\lambda_{\mathrm{ref}} - \lambda_1)}{(\lambda_2 - \lambda_1)} \quad (2)$$

The corrected radiance is the sum of the two terms:

$$L_{\mathrm{corr}}(\lambda_0) = L_{\mathrm{corr,irr}}(\lambda_0) + L_{\mathrm{corr,ref}}(\lambda_0) \quad (3)$$

Cell statistics

Mean command calculates the average of all input raster values. Resulted cloud average distribution is then converted into percentages raster based on 0 and 1 cloud probability. Classifying the final spatiotemporal cloud average distribution map was based on Jenks rule of classification, where Jenks rule identifies break points by picking the class breaks those best group similar values and heighten the differences between classes. The final output map was divided into three classes (1) not cloudy, (2) marginally cloudy and (3) cloudy.

Normalized difference water index

The normalized difference water index (NDWI) implemented in the current study practices: two near-InfraRed channels; one centered approximately at 0.86 μm, and the other at 1.24 μm represented as Near-Infrared (NIR) and Short Wave Infrared (SWIR) channels in Landsat 8, respectively. Following Cosh et al. (2013), as simple as NDVI, NDWI is defined as:

$$\mathrm{NDW\ I} = (1 - \mathrm{SWIR}/\mathrm{NIR})/(1 + \mathrm{SWIR}/\mathrm{NIR}) \quad (4)$$

To show that NDWI can be useful for remote sensing soil moisture status from space, the reflectance properties of green vegetation, dry vegetation and soils, and the absorption and scattering properties of atmospheric gases and aerosols were taken into consideration (Moghadas et al. 2013). Because the information about vegetation canopies contained in the SWIR channel is very different from that contained in the VIS channel, NDWI should be considered as an independent vegetation index (Palecki and Bell 2013). Integration of remote sensing applications and GIS proves to be a powerful tool in water resources management especially in arid environments (Youssef et al. 2012).

Results and discussion

Cloud detection algorithm was applied on 60 time series MERIS images and cloud detection thematic maps were produced. Three different masks were applied to verify the most certain method of cloud detection considered in the current research study. Thematic maps were summed and

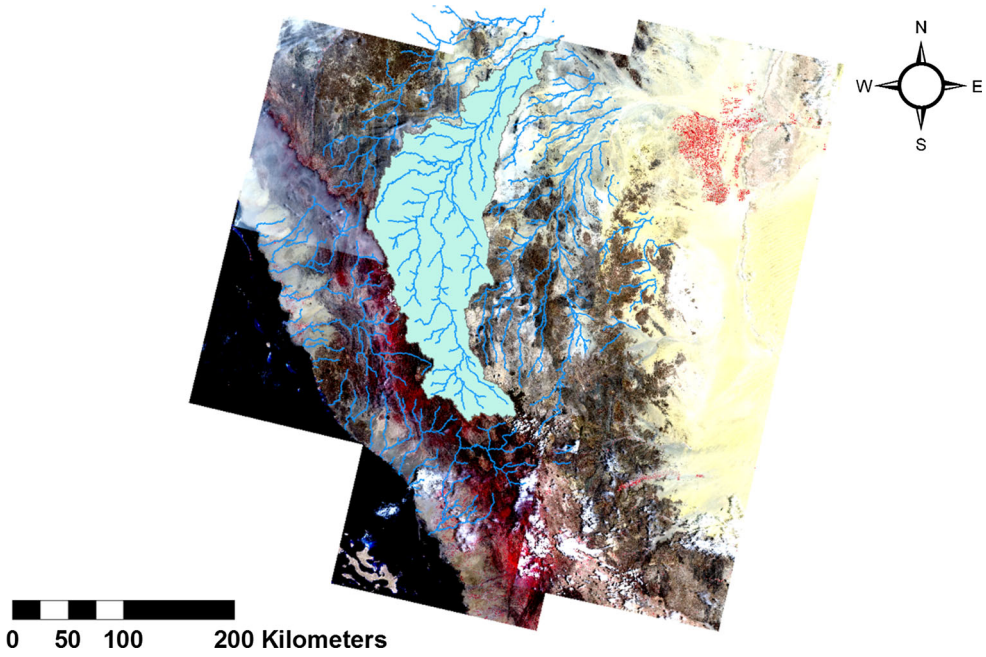

Fig. 3 Study area in false color composition with stream network illustrated

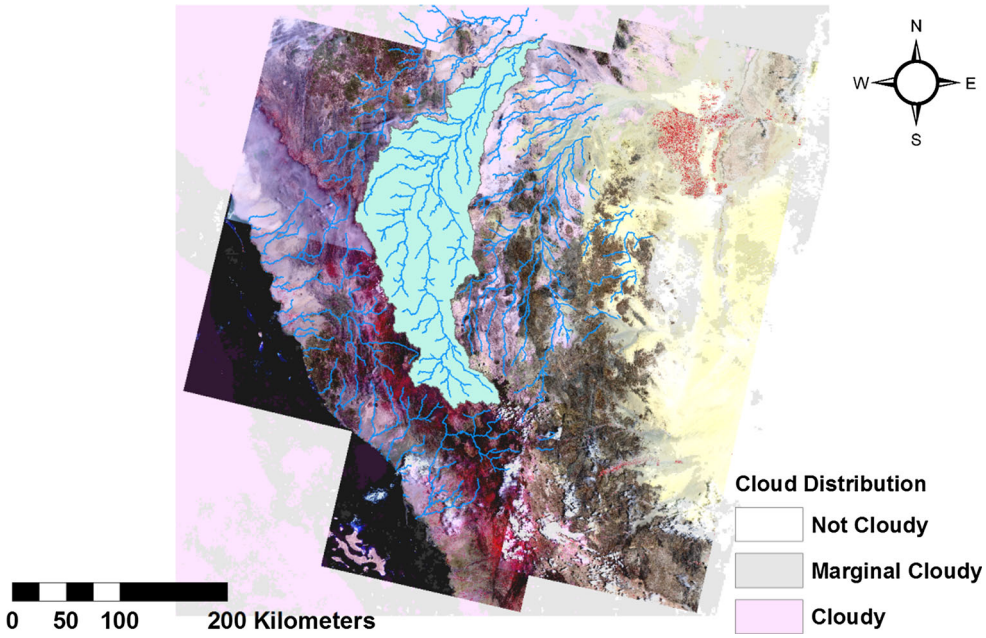

Fig. 4 Study area in false color composition with cloud coverage classes

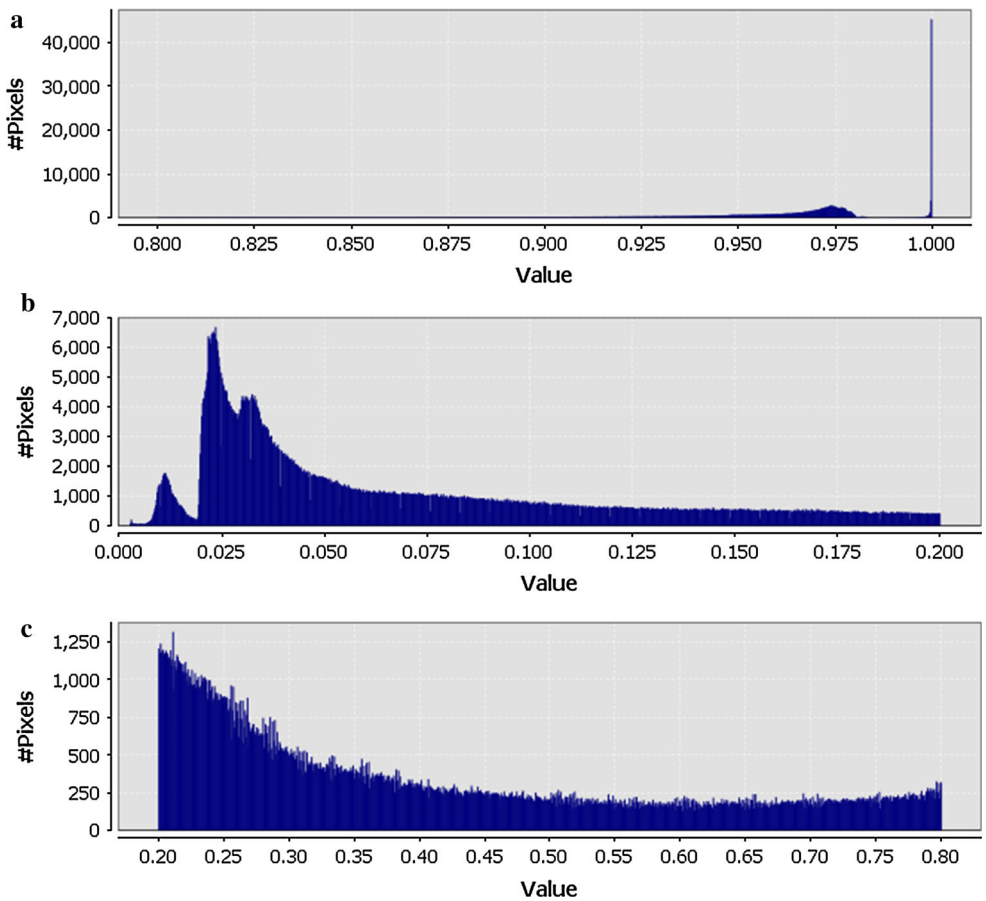

Fig. 5 **a** Stratocumulus clouds validation using cloudy mask, **b** stratocumulus clouds validation using cloud free mask, **c** stratocumulus clouds validation using cloud marginal mask

divided over 60 to produce average cloud spatiotemporal map. The use of 60 satellite images was considered as the minimum time series data set or model stability justification (Psilovikos and Elhag 2013).

Final cloud map was classified into three cloud status classes. The current algorithm verified to be resourceful in cloud detection over terrestrial landscape (Fischer and Bennartz 1997; Fischer et al. 1997; Key et al. 2004; Lindstrot

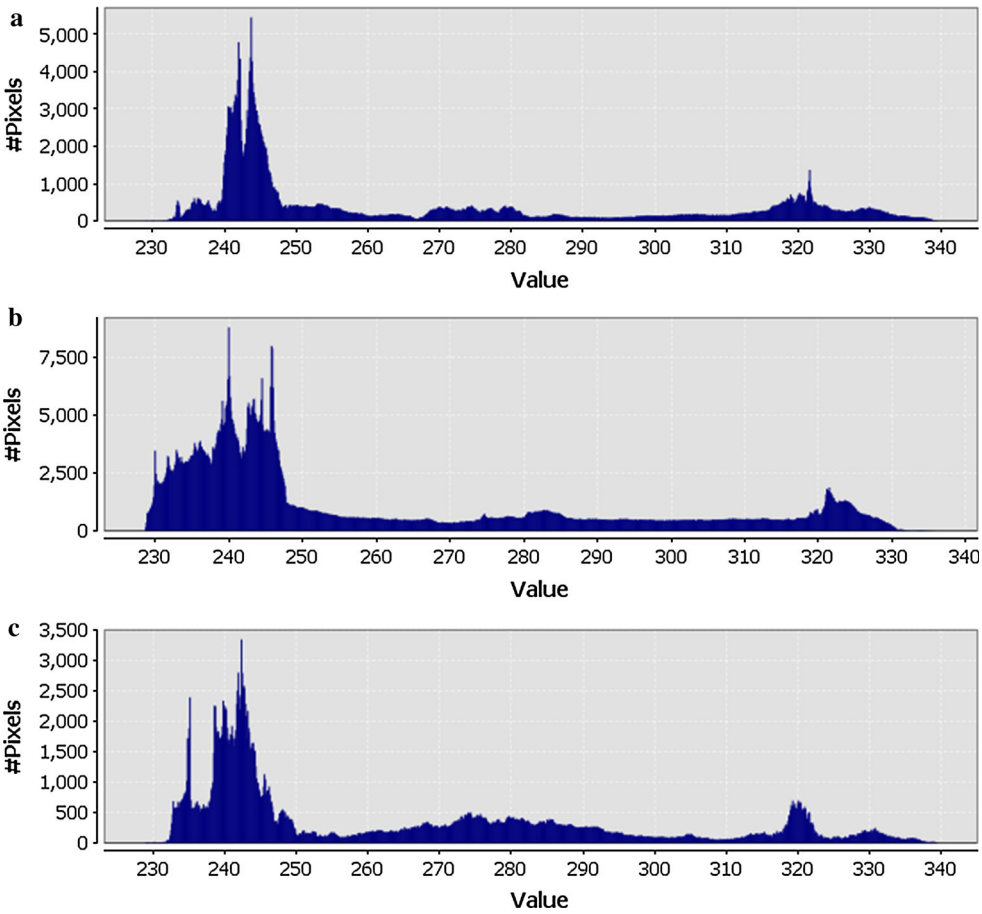

Fig. 6 **a** Total ozone validation using cloudy mask, **b** total ozone validation using cloud free mask, **c** total ozone validation using cloud marginal mask

et al. 2010). Watershed delineation resulted into several watershed exists in the study area, the uppermost surface runoff watershed is considered for further analysis in terms of water stream network (Fig. 3). Could spatiotemporal map illustrated in Fig. 4 shows the variation in terms of cloud cover, cloud certainty map emphasizes on some areas are always cloudy covered. Due to the mountain belt located in the study area, a cloud trap is also confined for certain areas most of the year. The western side of the watershed shares cloudy coverage most of the year with the mountain belt. This cloudy cover might be considered as the source of the watershed torrents (Ramos et al. 2011). Despite the fact that the majority of the selected watershed is either marginally cloudy or cloudy free; however, the sink of the watershed is covered mostly by clouds. Unanticipated flood incidents may lead to destructive impacts due to the geomorphological features in the study area (Youssef and Maerz 2013).

To illustrate the classification accuracy at individual images, cloud probability maps of the considered method are compared against the accuracy of the 'BEAM Cloud Probability Processor Flag' (stratocumulus clouds, total ozone concentration and relative humidity), which is the most acceptable reference providing a more accurate cloud mask than the official MERIS L1b and L2 products (Gomez-Chova et al. 2007; Guan et al. 2010).

Three different validation masks used against the three levels of cloud coverage, respectively (cloudy, marginal cloudy and not cloudy). Cloud mask illustrated distinct separation method of different cloud coverage; the value of the cloudy pixels was mostly at value 1 (Fig. 5a). Stratocumulus clouds validation was not distinct in Figs. 5b and 6c where the higher number pixels were kept at low pixel values (Frey et al. 2008). The use of total ozone concentration as validation mask demonstrated in Fig. 6a–c shows that the ozone mask is not the proper mask to validate cloudy pixels (Delwart et al. 2007; Engelhardt et al. 2013). Sharp peaks of ozone validation masks where for marginal cloud coverage class (Fig. 6b). In general term, ozone validation mask is the most proper mask to distinguish uncertain cloud pixels (King et al. 1992). Relative humidity validation mask showed a wide range of pixels values at the three cloud coverage classes (Fig. 7a–c). The mask is not distinguishing any class in particular; therefore, the use of the mask is not recommended for the BEAM Cloud Probability Processor (Goodman and Henderson-Sellers 1988; Simpson et al.

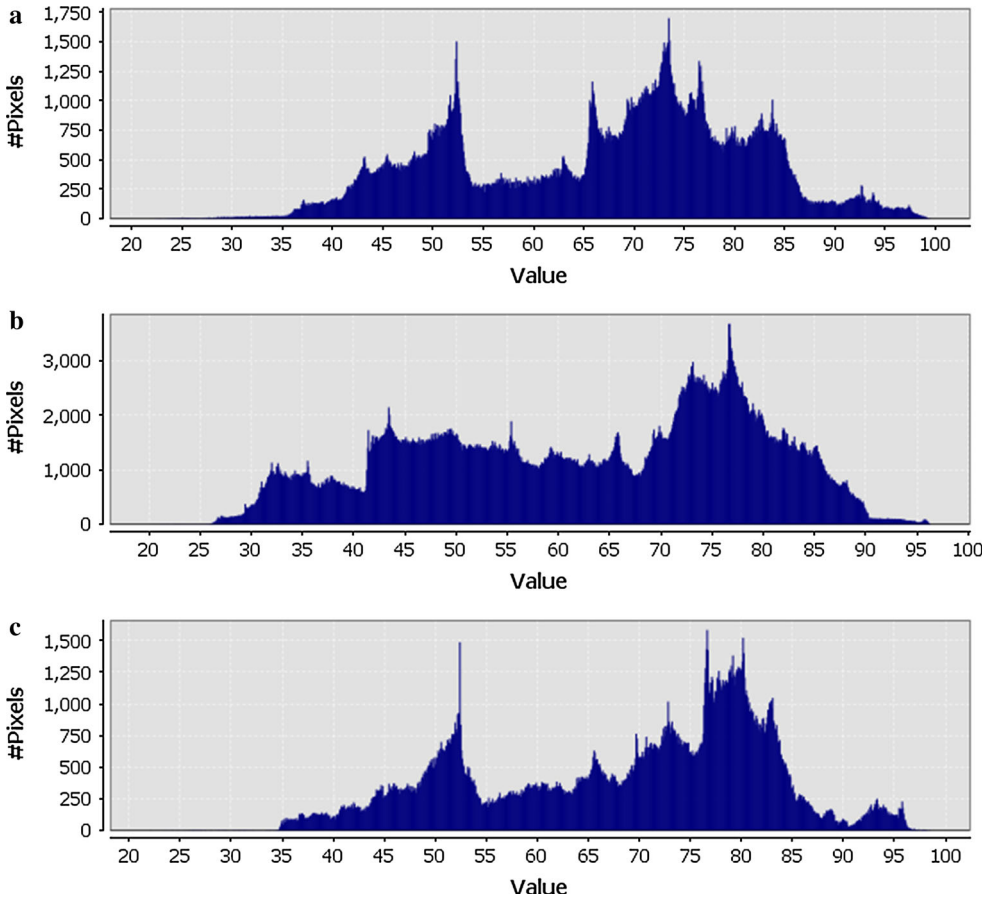

Fig. 7 **a** Relative humidity validation using cloudy mask, **b** relative humidity validation using cloud free mask, **c** relative humidity validation using cloud marginal mask

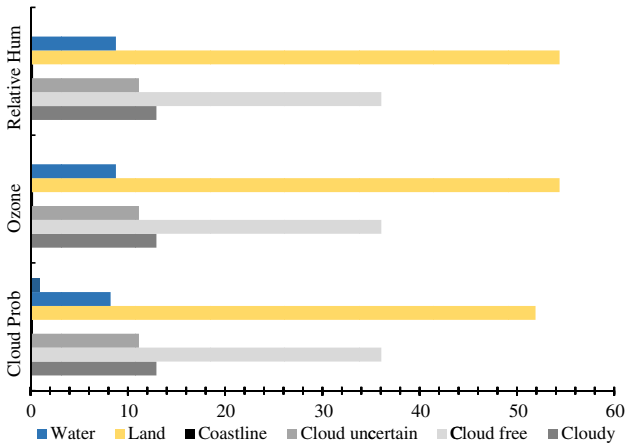

Fig. 8 Comparison chart of different land/cloud cover classes

1998). Further investigations based on the type of the clouds might be needed to fine tune the relative humidity mask (Molders et al. 1995; Key et al. 2004).

Figure 8 shows a comparison chart of different land/cloud cover classes, where the proposed algorithm (*y*-axis) clearly outperforms the selected reference independently of whether they were represented in the training set or not; and the proposed algorithm mainly provides validation values over 0.8 while the reference algorithm provides validation values between 0 and 1 (Gallaudet and Simpson 1991; Mecikalski et al. 2013).

Selected watershed located within Precambrian geological feature which is not adequate for groundwater recharge purposes due to the permeability of Precambrian layer, the watershed is deliberated as low permeable layer (Selaolo 1998; De Vries et al. 2000; El-Bastawesy et al. 2013). In contrary, only a small lower part of the watershed lies over a Quaternary alluvial geological layer which is characterized by higher permeability (De Vries 1997; Selaolo 1998; De Vries et al. 2000); the sink of the watershed receives the runoff and settled it down leaving a better chance for groundwater recharge process showed in Fig. 9 (El-Hames et al. 2011).

NDWI illustrated in Fig. 10 is indicating that the most of the eastern mountain belts of the study area including the designated watershed are located over a relatively dry soil. Dry soils have a higher tendency to accommodate preferably surface water which may lead to improve groundwater recharge (Tyler et al. 1996; Cobet 2000; De Vries et al. 2000; Brunner et al. 2007). Differences in spatial soil moisture content maps can be used for the

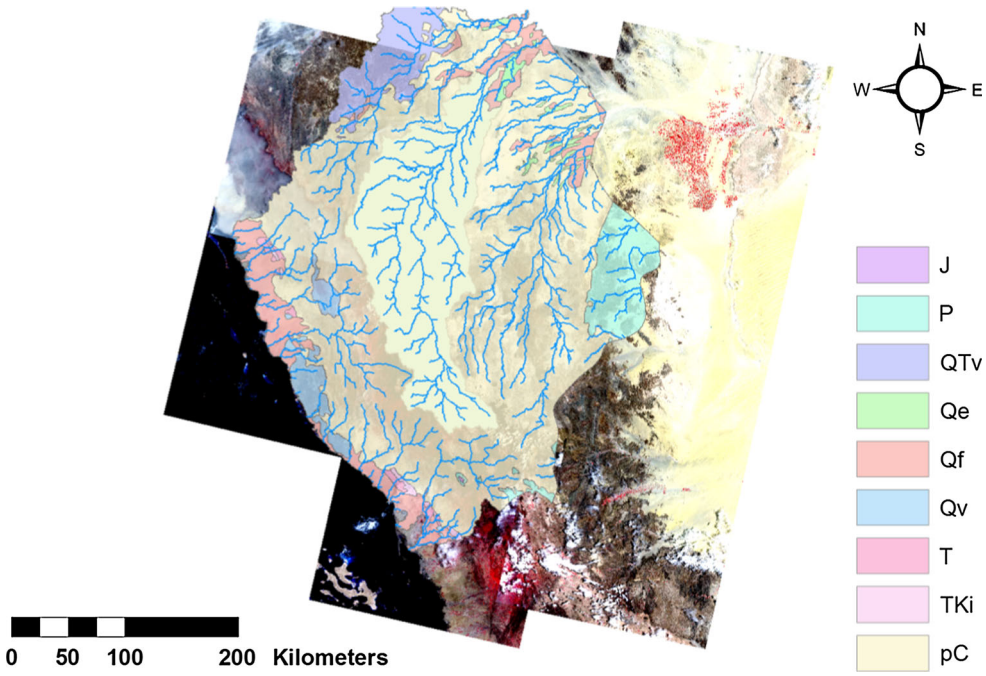

Fig. 9 Geological features of the study area within the designated watershed

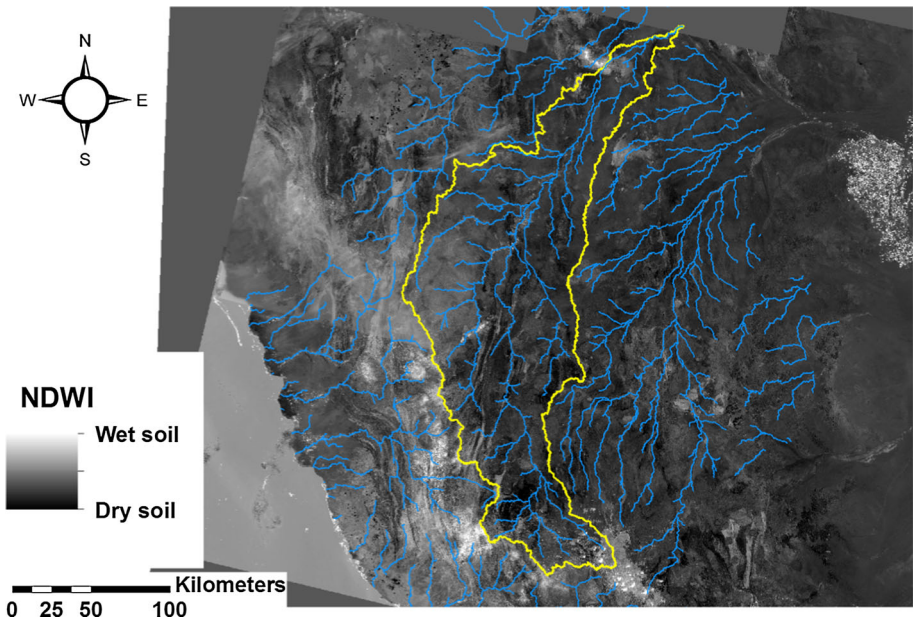

Fig. 10 Normalized difference water index map of the study area

identification of distinctive areas of potential for groundwater recharge (Roerink et al. 2000; Palecki and Bell 2013).

The main finding of the current research is based on the interconnections between the previously conducted results as it composed in Fig. 11, cloud coverage distribution map intersected with the geological map of the designated area. Furthermore, the stream network within the main watershed of the area draws the attention to the watershed sink to maximize the use of the rainwater and prevent frequent flood risks (Dawod et al. 2012). The sink is characterized by cloudy sky most of the year, relatively semi dry soil and adequate geological permeable layer (Chowdhury et al. 2010; Moghadas et al. 2013). The interconnections of those conditions improve groundwater recharge process through less evaporation effect, slower saturation velocity and higher potential permeability, respectively (Beverly et al. 1999; Zhang et al. 1999; Gehrels 2000). Temporal changes in land use in the designated area move toward reclaiming lands for agricultural practices which put more pressure on

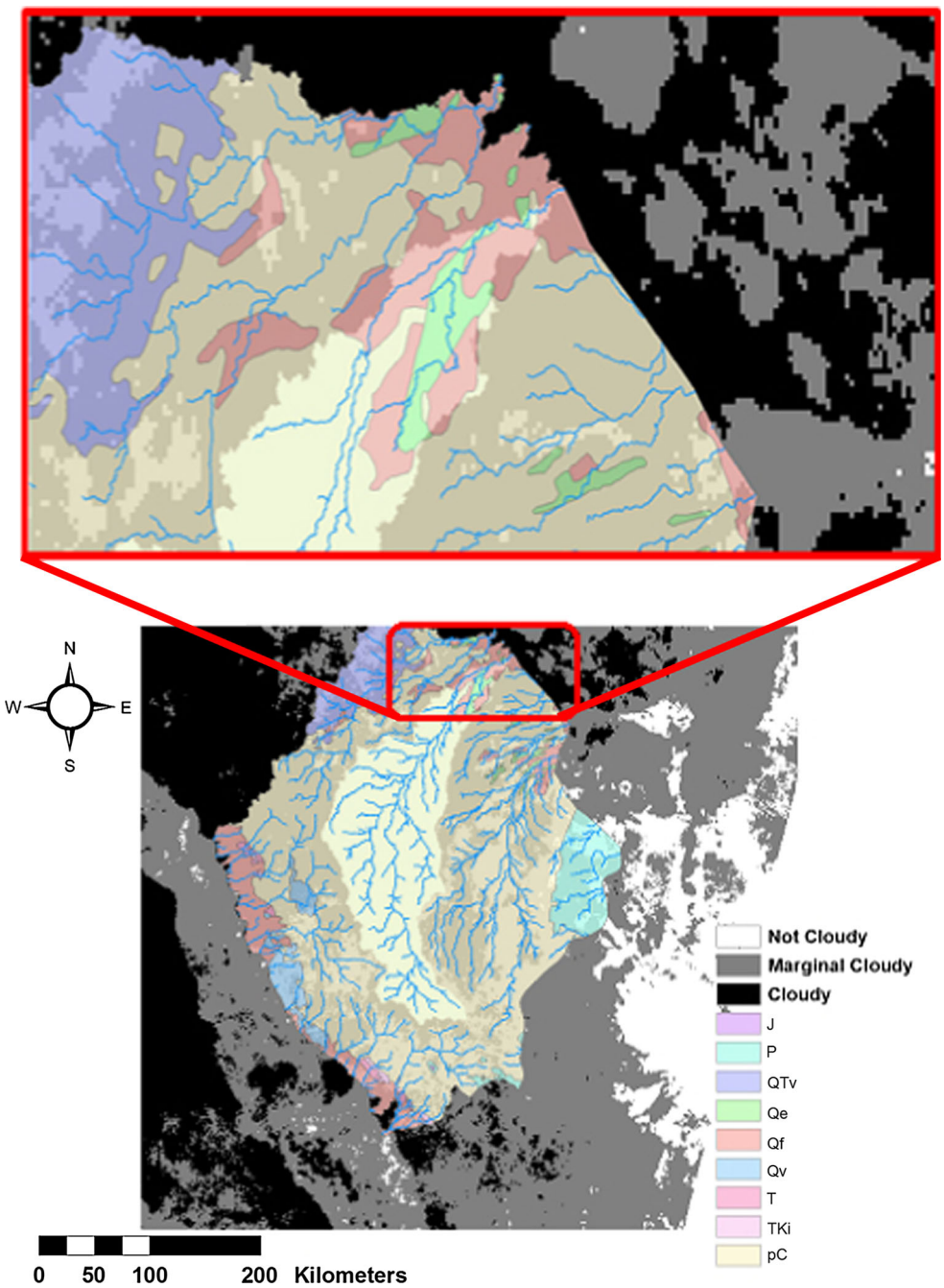

Fig. 11 Suggested area for groundwater recharge improvements

the scares water resources in such arid environment (Elhag et al. 2013).

Conclusions and recommendations

Determination of "hotspot" areas where the groundwater recharge potential is favorable is multi prospective process. Groundwater recharge is a complicated process and in general it is under studied in Saudi Arabia. Cloud detection algorithm showed robust results over different land covers within the study area, and the use of cloud probability validation mask proved to be the most preferable mask for cloud detection accuracy. Temporal cloud coverage analyses for 5 years period were conducted to assure the stability of the cloud disruption in arid environment. Presences of stable cloud coverage in some specific areas may reduce the surface runoff evaporation. Dry soils are more adequate to facilitate water percolation into deeper soils, wet soils are getting saturated rapidly and also may get clogged swiftly. The spatiotemporal distribution of the clouds raises the quest for the proper use of the current

methodology. The association concerning the cloudy pixels and type of geology feature beneath is the keystone of appropriate practice of the contemporary approach. Nevertheless, stratocumulus clouds are the main source of rainwater in the area so using the cloud coverage maps will be strongly exercising the conservational use of water resources management in arid regions. The practices of water resources management are many but the present methodology helps decision makers to decide where the dams need to be built to increase the potentials of groundwater recharge as a direct implementation of the adopted method from remote sensing data only when the limitation conditions are taken into account. Limiting conditions for the application of NDWI may rely mainly on surface roughness and the type of land use. The use of remote sensing data in terms of multi-spectral and multi-temporal imageries provides a cost-effective tool to obtain valuable information for better understanding and monitoring land development patterns and processes.

Acknowledgment This work was funded by the Deanship of Scientific Research (DSR), King Abdulaziz University, Jeddah, under grant No. (155-001-D1434). The authors, therefore, acknowledge with thanks DSR technical and financial support.

References

Al-Charideh A (2012) Recharge rate estimation in the mountain karst aquifer system of Figeh spring, Syria. Environ Earth Sci 65(4):1169–1178

Al-Othman AA, Ahmed I (2012) Hydrogeological framework and its implication on water level rise in Eastern ArRiyadh, Saudi Arabia. Environ Earth Sci 67(5):1493–1502

Beverly CR, Nathan RJ, Malafant KWJ, Fordham DP (1999) Development of a simplified unsaturated module for providing recharge estimates to saturated groundwater models. Hydrol Process 13:653–675

Brauman KA, Freyberg DL, Daily GC (2010) Forest structure influences on rainfall partitioning and cloud interception: a comparison of native forest sites in Kona, Hawaii. Agric For Meteorol 150:265–275

Brockmann C, Ruescas A, Stelzer K (2011) MERIS pixel identification. ATBD, ESA-ESRIN, pp 2–17

Bruijnzeel LA, Eugster W, Burkard R (2005) Fog as a hydrologic input. In: Anderson MG, McDonnell J (eds) Encyclopedia of hydrological sciences. John Wiley & Sons Ltd, Chichester, pp 559–582

Brunner P, Hendricks-Franssen HJ, Kgotlhang L, Bauer-Gottwein P, Kinzelbach W (2007) How can remote sensing contribute in groundwater modeling? Hydrogeol J 15(1):5–18

Chowdhury A, Jha MK, Chowdary VM (2010) Delineation of groundwater recharge zones and identification of artificial recharge sites in West Medinipur district, West Bengal, using RS, GIS and MCDM techniques. Environ Earth Sci 59(6):1209–1222

Cobet TF (2000) A groundwater-basin approach to conceptualize and simulate post-Pleistocene subsurface flow in a semi-arid region, southeastern New Mexico and western Texas, USA. Hydrogeol J 8(3):310–327

Cosh MH, Jackson TJ, Smith C, Toth B, Berg AA (2013) Validating the BERMS in situ soil water content data record with a large scale temporary network. Vadose Zone J. doi:10.2136/vzj2012.0151

Dasgupta S (2007) Remote sensing techniques for vegetation moisture and fire risk estimation. Ph.D. dissertation, George Mason University Virginia, United States

Dawod GM, Mirza MN, Al-Ghamdi KA (2012) GIS-based estimation of flood hazard impacts on road network in Makkah city, Saudi Arabia. Environ Earth Sci 67(8):2205–2215

De Vries JJ (1997) Prediction in hydrogeology: two case histories. Geol Rundsch 86:354–371

De Vries JJ, Selaolo ET, Beekman HE (2000) Groundwater recharge in the Kalahari, with reference to paleo-hydrologic conditions. J Hydrol 238:110–123

Deepika B, Avinash K, Jayappa KS (2013) Integration of hydrological factors and demarcation of groundwater prospect zones: insights from remote sensing and GIS techniques. Environ Earth Sci 70(3):1319–1338

Delwart S, Preusker R, Bourg L, Santer R, Ramon D, Fischer J (2007) MERIS inflight spectral calibration. Int J Remote Sens 28:479–496

El-Bastawesy M, Ali RR, Al Harbi K, Faid A (2013) Impact of the geomorphology and soil management on the development of waterlogging in closed drainage basins of Egypt and Saudi Arabia. Environ Earth Sci 68(5):1271–1283

Elhag M, Bahrawi J (2014) Cloud coverage disruption for groundwater recharge improvement using remote sensing techniques in Asir Region, Saudi Arabia. Life Sci J 11(1):192–200

Elhag M, Psilovikos A, Manakos I, Perakis K (2011) Application of the SEBS water balance model in estimating daily evapotranspiration and evaporative fraction from remote sensing data over the Nile Delta. Water Resour Manag 25(11):2731–2742

Elhag M, Psilovikos A, Sakellariou M (2013) Detection of land cover changes for water recourses management using remote sensing data over the Nile Delta Region. Environ Dev Sustain 15(5):1189–1204

El-Hames AS, Al-Ahmadi M, Al-Amri N (2011) A GIS approach for the assessment of groundwater quality in Wadi Rabigh aquifer, Saudi Arabia. Environ Earth Sci 63(6):1319–1331

El-Maghraby MS, Abu El Nasr AO, Hamouda MA (2013) Quality assessment of groundwater at south Al Madinah Al Munawarah area, Saudi Arabia. Environ Earth Sci 70(4):1525–1538

Engelhardt I, Rausch R, Keim B, Al-Saud M, Schuth C (2013) Surface and subsurface conceptual model of an arid environment with respect to mid- and late Holocene climate changes. Environ Earth Sci 69(2):537–555

Feister U, Möller H, Sattler T, Shields J, Görsdorf U, Güldner J (2010) Comparison of macroscopic cloud data from ground-based measurements using VIS/NIR and IR instruments at Lindenberg, Germany. Atmos Res 96:395–407

Fell F, Fischer J (2001) Numerical simulation of the light field in the atmosphere–ocean system using the matrix-operator method. J Quant Spectrosc Radiat Transf 3:351–388

Fischer J, Bennartz R (1997) Retrieval of total water vapour content from MERIS measurements, algorithm theoretical basis document PO-TN-MEL-GS-0005. ESA-ESTEC, Noordwijk

Fischer J, Grassl H (1984) Radiative transfer in an atmosphere ocean system: an azimuthally dependent matrix-operator approach. Applied Optics 23:1032–1041

Fischer J, Preusker R, Schüller L (1997) ATBD cloud top pressure. European Space Agency Algorithm Theoretical Basis Doc. PO-TN-MEL-GS-0006, p 28

Frey RA, Ackerman SA, Liu Y, Strabala KI, Zhang H, Key JR, Wang X (2008) Cloud detection with MODIS. Part I. Improvements in the MODIS cloud mask for collection 5. J Technol 25:1057–1072

Gallaudet TC, Simpson JJ (1991) Automated cloud screening of AVHRR imagery using split-and-merge clustering. Remote Sens Environ 38:77–100

Gehrels JC (2000) Recharge assessment: comparing tracers, micrometeorology and soil water models. In: Sililo O et al (eds) Groundwater: past achievements and future challenges. AA Balkema, Rotterdam, pp 147–152

Gieske ASM (1992) Dynamics of groundwater recharge: a case study in semi-arid eastern Botswana. PhD Thesis, Vrije Universiteit, Amsterdam, p 289

Gomez-Chova L, Camps-Valls G, Calpe J, Guanter L, Moreno J (2007) Cloud screening algorithm for ENVISAT/MERIS multispectral images. IEEE Trans Geosci Remote Sens 45(12):4105–4118

Goodman AH, Henderson-Sellers A (1988) Cloud detection analysis: a review of recent progress. Atmos Res 21:203–221

Guan NH, Zubir M, Jafri M, Abdullah K (2010) Improved cloud detection technique at South China Sea. Aerospace Technologies Advancements, SBN 978-953-7619-96-1, p 492

Hoetzl H (1995) Groundwater recharge in an arid karst area (Saudi Arabia). Int Assoc Hydrol Sci 232:195–207

Holder CD (2003) Fog precipitation in the Sierra de las Minas Biosphere Reserve, Guatemala. Hydrol Process 17:2001–2010

Holder CD (2004) Rainfall interception and fog precipitation in a tropical montane cloud forest of Guatemala. For Ecol Manag 190:373–384

Huang CC, Yeh HF, Lin HI, Lee ST, Hsu KC, Lee CH (2013) Groundwater recharge and exploitative potential zone mapping using GIS and GOD techniques. Environ Earth Sci 68(1):267–280

Jedlovec GJ, Haines SL, LaFontaine FJ (2008) Spatial and temporal varying thresholds for cloud detection in GOES imagery. IEEE Trans Geosci Remote Sens 46(6):1705–1717

Kazantzidis A, Tzoumanikas P, Bais AF, Fotopoulos S, Economou G (2012) Cloud detection and classification with the use of whole-sky ground-based images. Atmos Res 113:80–88

Key EL, Minnett PJ, Jones RA (2004) Cloud distributions over the coastal Arctic Ocean: surface-based and satellite observations. Atmos Res 72(1–4):57–88

King MD, Kaufman YJ, Menzel WP, Tanré D (1992) Remote sensing of cloud, aerosol, and water vapor properties from the moderate resolution imaging spectrometer (MODIS). IEEE Trans Geosci Remote Sens 30:1–27

Lindstrot R, Preusker R, Fischer J (2009) The retrieval of land surface pressure from MERIS measurements in the Oxygen A band. J Atmos Ocean Technol 26:1367–1377

Lindstrot R, Preusker R, Fischer J (2010) The empirical correction of stray light in the MERIS oxygen A band channel. J Atmos Ocean Technol 27(7):1185–1194

McNally AP, Watts PD (2003) A cloud detection algorithm for high spectral resolution infrared sounders. Q J R Meteorol Soc 129:3411–3423

Mecikalski JR, Watts D, Koenig M (2011) Use of Meteosat Second Generation optimal cloud analysis fields for understanding physical attributes of growing cumulus clouds. Atmos Res 102(1–2):175–190

Mecikalski JR, Minnis P, Palikonda R (2013) Use of satellite derived cloud properties to quantify growing cumulus beneath cirrus clouds. Atmos Res 120–121:192–201

Moghadas D, Jadoon KZ, Vanderborght J, Lambot S, Vereecken H (2013) Effects of near surface soil moisture profiles during evaporation on far-field ground-penetrating radar data: a numerical study. Vadose Zone J. doi:10.2136/vzj2012.0138

Molders N, Laube M, Raschke E (1995) Evaluation of model generated cloud cover by means of satellite data. Atmos Res 39(1–3):91–111

Palecki MA, Bell JE (2013) U.S. Climate Reference Network soil moisture observations with triple redundancy: measurement variability. Vadose Zone J. doi:10.2136/vzj2012.0158

Prada S, Menezes de Sequeira M, Figueira C, Prior V, Silva MO (2010) Response to "comment on fog precipitation and rainfall interception in the natural forests of Madeira Island (Portugal)". Agric For Meteorol 150:1154–1157

Prada S, Menezes de Sequeira M, Figueira C, Silva MO (2009) Fog precipitation and rainfall interception in the natural forests of Madeira Island (Portugal). Agric For Meteorol 149:1179–1187

Psilovikos A, Elhag M (2013) Forecasting of remotely sensed daily evapotranspiration data over Nile Delta Region, Egypt. Water Resour Manag 27(12):4115–4130

Ramos AM, Ramos R, Sousa P, Trigo RM, Janeira M, Prior V (2011) Cloud to ground lightning activity over Portugal and its association with circulation weather types. Atmos Res 101(1–2):84–101

Rink K, Kalbacher T, Kolditz O (2012) Visual data exploration for hydrological analysis. Environ Earth Sci 65(5):1395–1403

Roerink GJ, Su Z, Mementi M (2000) S-SEBI: a simple remote sensing algorithm to estimate the surface energy balance. Phys Chem Earth Part B 2(2):147–157

Saunders RW, Kriebel RT (1988) An improved method for detecting clear sky and cloudy radiances from AVHRR data. Int J Remote Sens 9:123–150

Selaolo ET (1998) Tracer studies and groundwater recharge assessment in the eastern fringe of the Botswana Kalahari. PhD thesis, Vrije Universiteit, Amsterdam, p 229

Simpson JJ, Schmidt AB, Harris A (1998) Improved cloud detection in along track scanning radiometer (ATSR) data over the ocean. Remote Sens Environ 65:1–24

Tyler SW, Chapman JB, Conrad SH, Hammermeister DP, Blout DO, Miller JJ, Sully MJ, Ginanni JM (1996) Soil-water flux in the Southern Great Basin, United States: temporal and spatial variations over the last 120,000 years. Water Resour Res 32:1481–1499

Weaver C, Ginoux P, Hsu C, Chou M, Joiner J (2001) Radiative forcing of Saharan dust. GOCART model simulations compared with ERBE data. J Atmos Sci 59(3):736–747

Youssef AM, Maerz NH (2013) Overview of some geological hazards in the Saudi Arabia. Environ Earth Sci 70(7):3115–3130

Youssef AM, Pradhan B, Sabtan AA, El-Harbi HM (2012) Coupling of remote sensing data aided with field investigations for geological hazards assessment in Jazan area, Kingdom of Saudi Arabia. Environ Earth Sci 65(1):119–130

Zhang L, Dawes WR, Hatton TJ, Reece PH, Beale GTH, Packer I (1999) Estimation of soil moisture and groundwater recharge using the TOPOG_IRM model. Water Resour Res 35(1):149–161